Passive seismic monitoring of carbon dioxide storage at Weyburn

James P. Verdon and J-Michael Kendall, University of Bristol
Don J. White, Geological Survey of Canada
Doug A. Angus and Quentin J. Fisher, University of Leeds
Ted Urbancic, Engineering Seismology Group Canada

Carbon capture and storage (CCS) is currently one of several candidate technologies for reducing the emission of industrial CO_2 to the atmosphere. As plans for large-scale geological storage of CO_2 are being considered, it is clear that monitoring programs will be required to demonstrate security of the CO_2 within the storage complex. Numerous geophysical monitoring techniques are currently being tested for this purpose, including controlled-source time-lapse reflection seismology, satellite synthetic aperture radar interferometry, electromagnetic sounding, gravity, and others. Passive seismic monitoring is an additional technique under consideration that complements these other techniques, and has potential as a cost-effective method of demonstrating storage security. This is particularly true over longer periods of time, as passive seismic arrays cost relatively little to maintain. Of the large-scale CCS pilot projects currently operational, thus far only the IEA GHG Weyburn-Midale CO_2 Monitoring and Storage Project has included passive seismic monitoring. Here we present the results from five years of passive seismic monitoring at Weyburn, and discuss the lessons learnt that can be applied when deploying passive seismics to monitor future CCS operations.

Figure 1. *Location of the Weyburn Field, set in the Williston Basin in central Canada.*

Passive seismic monitoring

Activities such as production of hydrocarbons or injection of CO_2 will alter the pore pressure, and therefore the effective stresses, both inside and around a reservoir. This can lead to the reactivation of pre-existing faults and fractures, or even the formation of new fault/fracture networks. Fracture formation and fault movements can emit seismic energy, which is recorded on geophones installed in boreholes near the reservoir. Various methods exist to locate event hypocenters based on the energy recorded at the geophones, many of which have their basis in global seismological research. Accurate location of events can identify active fault planes, and identification of focal mechanisms can reveal the style and orientation of deformation (e.g., Rutledge et al., 2004). Furthermore, as the seismic energy recorded has usually travelled exclusively through rock in or near the reservoir, wave-propagation effects such as S-wave splitting can provide direct information about features in the reservoir, such as the presence of aligned fractures and reservoir quality (e.g., Verdon et al. 2009).

Passive seismic monitoring provides a different kind of information to controlled-source techniques. Recording is continuous, and information can be analyzed in near real time. Yet the technique can only image areas between where microseismic events are occurring and receivers are located. Furthermore, since the locations of microseismicity vary spatially, using temporal variations of microseismicity to monitor fluid-related velocity changes is challenging. Whilst 4D controlled-source seismics are sensitive to changes in fluid saturation and stresses, passive seismic monitoring is an excellent technique for identifying geomechanical deformation induced by injection. The detection of active faults and fractures or new fractures generated within the cap rock of a reservoir is important for CCS because these may provide pathways for CO_2 leakage, especially if they propagate far into the overburden. Furthermore, once geophones have been installed, the costs of maintenance and data processing are small in comparison with controlled-source seismic techniques. This is an important consideration for CCS where a site may need to be monitored long after injection has ceased and the field shut in.

Overview of the Weyburn-Midale project

The Weyburn-Midale Field is in the Williston Basin of southern Saskatchewan, Canada (Figure 1). A schematic view of the reservoir is shown in Figure 2. The reservoir is in the Carboniferous Midale beds at depths of ~1430 m. It consists of fractured lower limestone (vuggy unit) and upper dolomite (marly unit) layers, with a total thickness of ~30 m, overlain by an anhydrite caprock. An important secondary seal is provided by the Lower Watrous member, which constitutes a thick layer of shale-rich Mesozoic sediments that lie just above the reservoir. The field has been in production since 1954; initial waterflooding commenced in the

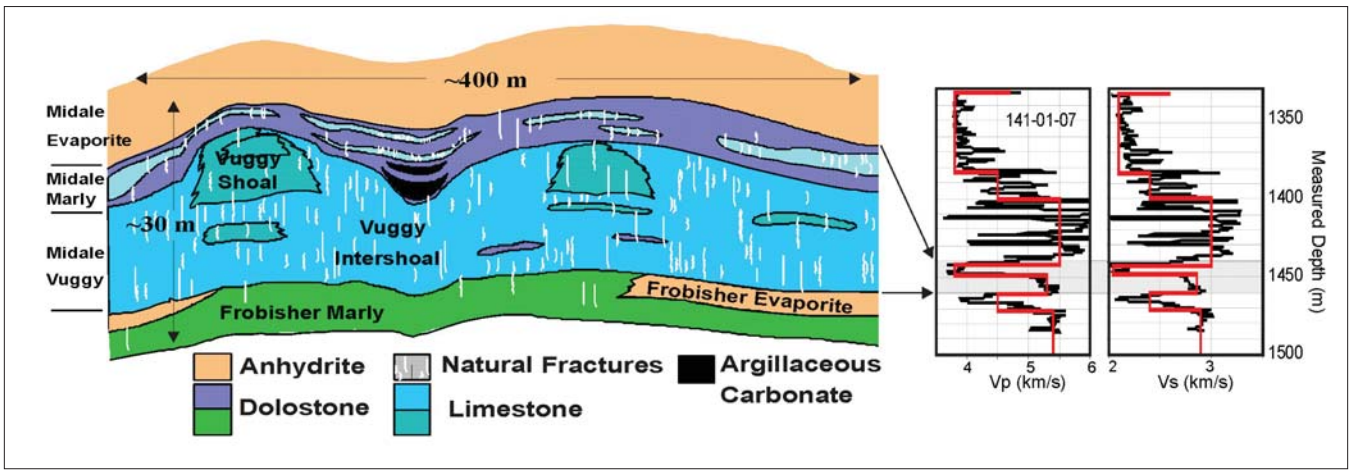

Figure 2. *Schematic cross section through the Weyburn reservoir, showing the lower vuggy and upper marly units (from Wilson et al., 2004). The primary seal is the Midale evaporite, whilst an important secondary seal is the unconformably overlying Watrous member (not shown) of Jurassic age. The P- and S-wave velocity models used for event location are on the right; the logs (from well 141/01-07) are black whereas the blocked velocity models are red.*

1960s, and horizontal infill wells were drilled in the 1990s. CO_2 injection was initiated in 2000 to enhance oil recovery, resulting in production levels last seen in the mid-1970s. However, a research component was also included to test and develop techniques for monitoring large volumes of CO_2 in the subsurface. Current injection rates are over 3 million tonnes of CO_2 per year in the Weyburn-Midale Field—the equivalent to CO_2 emissions from ~400,000 cars. Injection rates for individual wells range from 50 to 500 tonnes per day. Controlled-source 4D seismic monitoring has been largely successful in imaging the plumes of CO_2 migrating away from the injection wells, with negative time-lapse amplitude differences marking zones of CO_2 saturation (White, 2009).

Passive monitoring at Weyburn has focused on a single pattern within the field. In 2003, a passive recording array consisting of 8 triaxial 20-Hz geophones was cemented in an inactive vertical well within 50 m of a planned new vertical CO_2 injection well (121/06-08). The layout of injection, production, and monitoring wells can be seen in Figure 3. Geophones were spaced at intervals of 25 m between depths of 1181 and 1356 m, roughly 200 m above the reservoir. The system was operated in "triggered" mode, using a trigger window length of 200 ms and requiring processed signal levels exceeding threshold on 5 of the 8 geo-

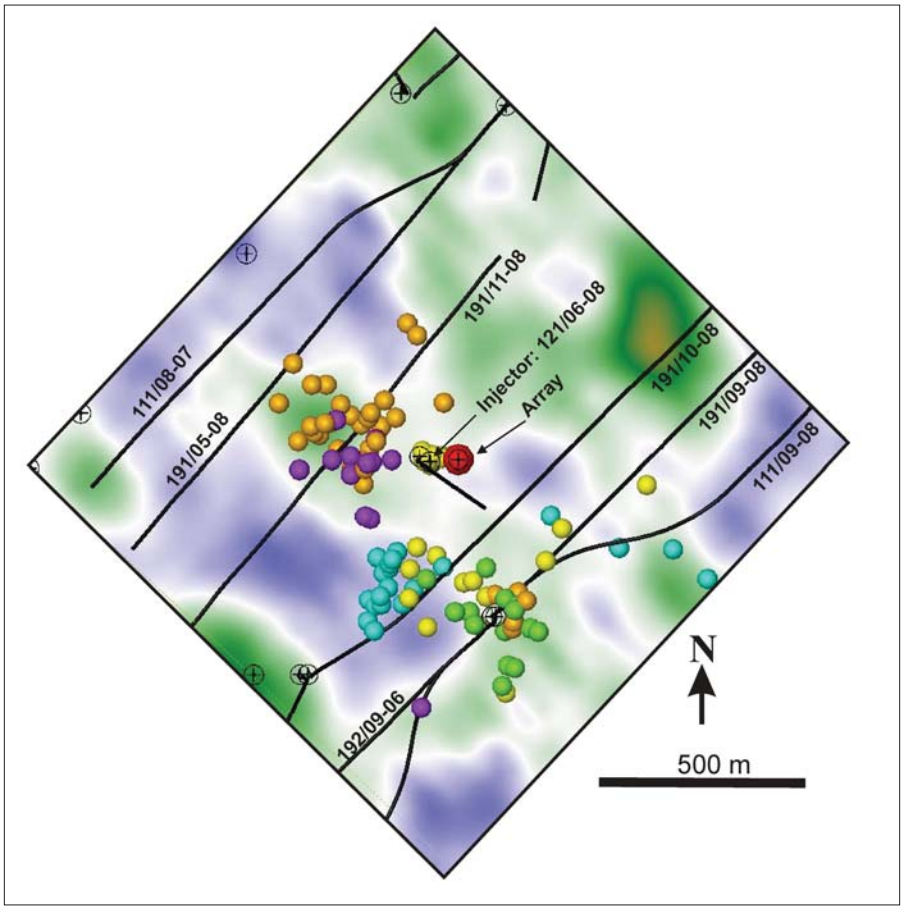

Figure 3. *Microseismic event locations from August 2003 to January 2006, superposed on the 2004 time-lapse amplitude difference map (from 4D surface seismic). Green-to-orange and blue background colors represent negative and positive differences, respectively. The amplitude differences represent the 2004 minus the 2000 amplitudes where the amplitudes in each case represent the arithmetic mean for a 5-ms window centered on the Midale marly horizon. The Midale marly unit is a low-impedance interval and thus negative time-lapse amplitude differences represent zones where the impedance has been further reduced by the presence of CO_2. Event clusters are color-coded according to time intervals: pre-injection period (yellow); initial injection (purple); production well shut-in 18–19 March 2004 (green); high-injectivity period (orange); low-frequency events during January 2006 (light blue). The locations of the injection, production, and monitoring wells are also marked.*

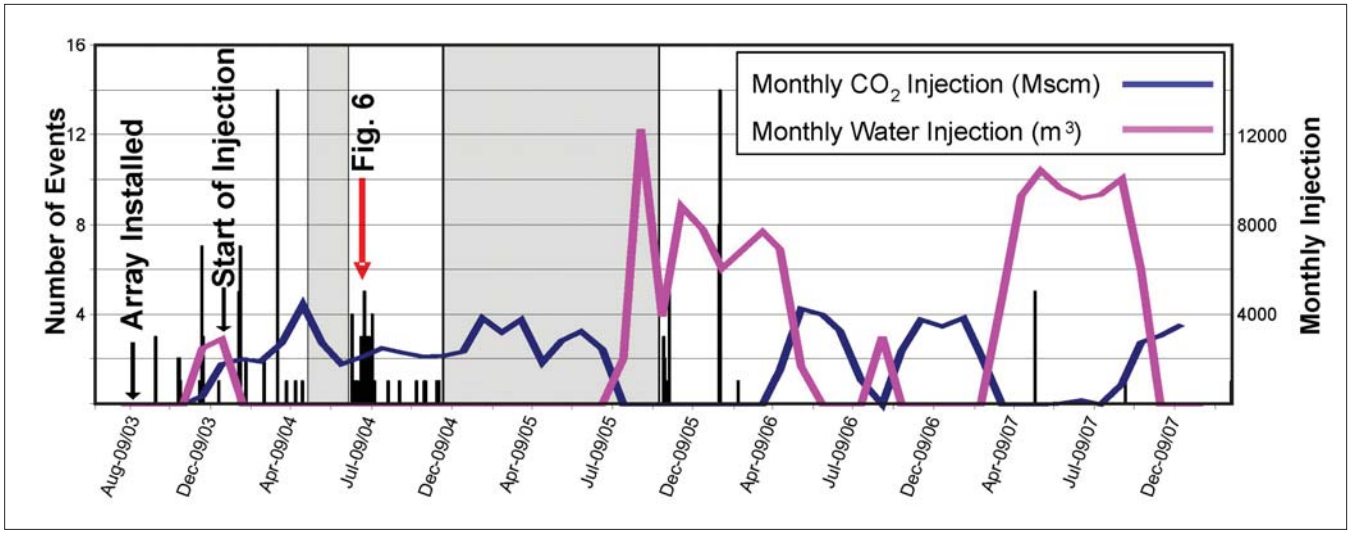

Figure 4. *Histogram of located microseismic events from August 2003 to January 2008. Also shown are the monthly injection volumes for the WAG injection program in vertical well 121/06-08. The gray shaded areas indicate periods when the passive array was not recording.*

phones for event triggering and data storage to be initiated. Passive monitoring commenced in August 2003, prior to the onset of water injection in December 2003, and has been in semi-continuous operation to present with the exception of an 11-month downtime from December 2004 to October 2005 (Figure 4). During this period, approximately 100 locatable microseismic events have been recorded, documenting a low rate of low-intensity events. Figure 5 shows event moment magnitudes for the same events as a function of distance from the array. The majority of events have moment magnitudes between -3.0 and -1.0. This plot suggests that surface arrays would have limited use for microseismic monitoring under conditions like Weyburn. The largest events recorded have a moment magnitude of less than –1.0, and most events are smaller than –2.0. Dense surface arrays would be required to detect such events, and their detectability would be strongly influenced by surface noise and the nature of the event focal mechanisms. Dominant frequencies of up to 150 Hz are observed for some of the more impulsive events. However, the majority of events are characterized by frequencies closer to the 20-Hz resonant frequency of the geophones, leading to relatively large uncertainties in the locations. Events have been located up to ~500 m from the geophones.

Water injection in the nearby 121/06-08 vertical injection well began on 15 December 2003 with a switch over to CO_2 on 22 January 2004. Injection has continued under a WAG (water-alternating-gas) process (Figure 4).

Event locations

Microseismic event hypocenters were determined by matching the observed P- and S-wave arrival times by ray tracing, and determining the propagation azimuth by hodogram analysis across the levels of the array. A one-dimensional velocity model (Figure 2) was adopted for the purposes of ray tracing based on a dipole sonic log. Sensitivity of event locations to the velocity model was examined by varying velocities by ±250 m/s, with resultant location changes of 75

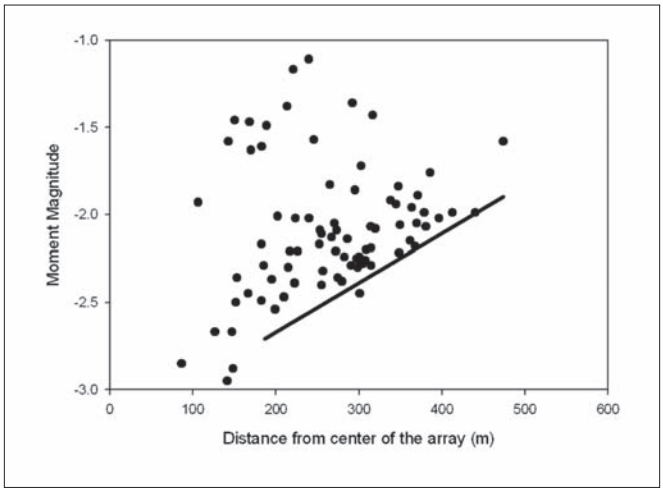

Figure 5. *Magnitude versus distance plot for events up to July 2004.*

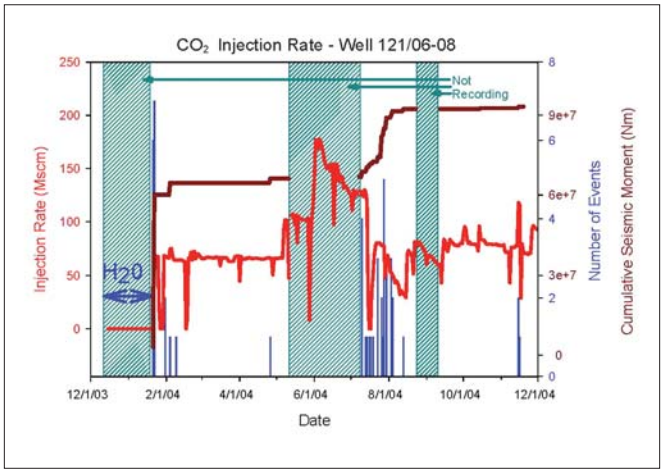

Figure 6. *Daily CO_2 injection volume (red), histogram of microseismic events (blue), and calculated cumulative seismic moment (maroon) for injection well 121/06-08. The period of high injection runs from May to July 2004, with elevated microseismic rates continuing through August 2004.*

m NS, 20 m EW and 70 m vertically. In addition, errors in location are as high as several hundred meters in cases where the P- and S-phase onsets are emergent or poorly defined.

The located events between August 2003 and January 2006 are plotted in Figure 3, with temporal clusters of events grouped by color. Before injection began, approximately 30 events were recorded. Most of these are related to completion activities in the injection well, which in Figure 3 form a tight cluster of yellow dots centered on the injector. The remaining events (yellow dots) form a diffuse distribution near horizontal production wells (191/09-08 and 191/10-08). Similar events were recorded at various times during the overall monitoring period, including a cluster of 15 events (green dots) occurring on 18–19 March 2004 during well shut in. These events are characterized by good signal-to-noise levels and relatively high frequencies (up to 150 Hz). The timing of these events correlates directly with periods when the production wells are shut-in, and thus are likely associated with local pressure recovery during shut-in that leads to shear failure.

Water injection began on 15 December 2003. The resultant increase in background noise levels caused the microseismic system to trigger continuously and then shut down until 12 January 2004, meaning that no data were acquired during this period. Water injection stopped in well 121/06-08 on 22 January at 8 a.m., and CO_2 injection started the same day at 11 a.m. On 21 January and 22 January, 13 events (purple dots in Figure 3) were recorded, *before the start of CO_2 injection*. They form a spatial cluster that extends up to 300 m east of the injector toward production well 191/11-08. In contrast to the pre-injection events near production well 191/09-08, these events are characterized by relatively low-peak frequencies (20–30 Hz) and short separation between P- and S-waves making hypocentral location difficult and leading to large location uncertainties. The relatively low frequencies of these events suggests that the inducing mechanism is gas or fluid movement. However, in that the events all occur prior to the onset of CO_2 injection, they clearly are associated with the movement of fluids other than CO_2.

The rate of CO_2 injection in 121/06-08 was increased by almost a factor of 2 for a period of eight weeks from early May to July 2004 (see Figure 6). The seismic array was only operational during the latter stages of this period. Microseismicity continued past the increased injection period for almost four weeks, and 34 events were located. The cluster of events (orange dots, Figure 3) continues the trend defined by the injection-related events of 21–22 January 2004 (purple dots, Figure 3). We note that this cluster correlates well with a negative lobe in the 2004–2000 time-lapse seismic map, marking a region of CO_2 saturation

The last significant group of microseismic events occurred during 17–18 January 2006 when a total of 20 events occurring over a period of four hours were detected and located (light blue dots in Figure 3). These events have characteristically low frequencies similar to the events recorded near the start of CO_2 injection. Since January of 2006, there have been fewer than 10 locatable microseisms. This paucity in microseismic activity may be real or could potentially be due to a reduced sensitivity of the recording array or increased noise levels over time.

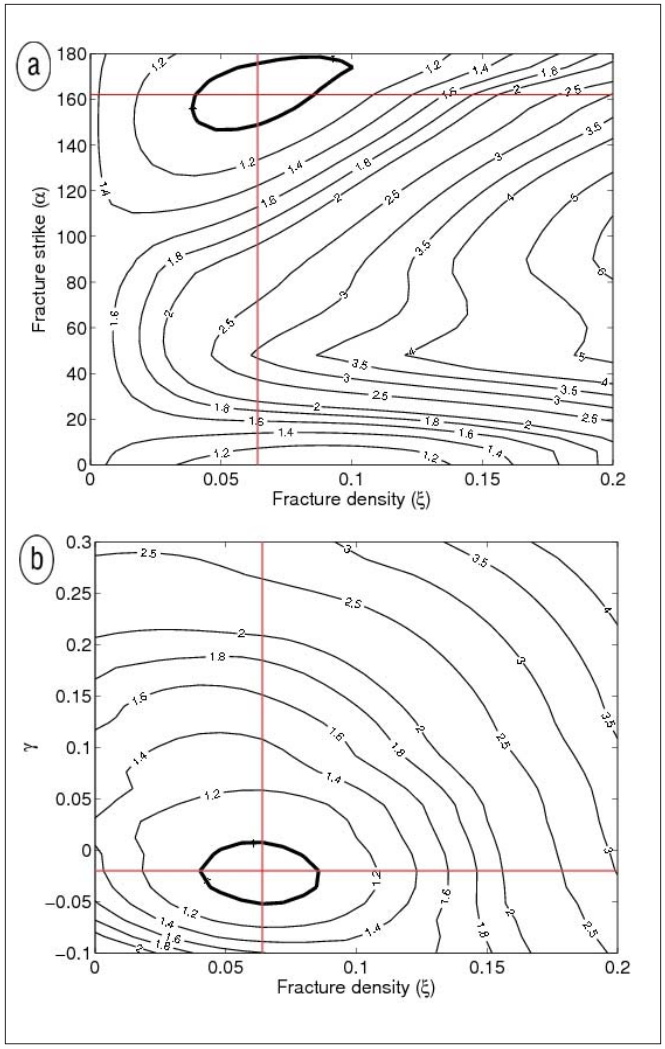

Figure 7. *Results from the inversion of splitting measurements for fracture properties, showing the rms misfit as a function of (a) fracture strike and density at best-fit sedimentary fabric strength (Thomsen's γ parameter), and (b) the best-fit fracture density and sedimentary fabric at the best-fit fracture strike. The 90% confidence interval is marked by the bold lines, and the best-fit model by the red lines. The inversion finds a low value for γ (as observed in core samples), and a fracture set striking to the NW with fracture density between 0.05 and 0.1.*

S-wave splitting

The energy recorded on the geophones has travelled through rocks in and around the reservoir. Therefore, any wave propagation effects can be used to make inferences about the properties of these rocks. S-wave splitting is particularly useful, as it allows the direct measurement of anisotropy, which may indicate the presence of sedimentary layering or aligned fractures. Forward modeling using rock physics theory can be used to find the combinations of fracture geometries and sedimentary fabrics that best fit the observed splitting measurements (see Verdon et al., 2009).

The data from Weyburn were analysed for S-wave splitting using a semi-automated approach. Interpretation of

splitting measurements from rays that have travelled obliquely through the reservoir is not intuitive, as both sedimentary fabrics and fractures influence time-lags and fast directions in a directionally dependent and nonlinear manner. It is therefore necessary to develop rock physics models that invert splitting measurements from many arrival angles for fracture geometries. The free parameters used in our inversion are the Thomsen parameters γ and δ (giving the strength of a vertically transverse isotropy or VTI sedimentary fabric), and the strike and density of a set of vertical, aligned fractures α and ξ, respectively. We plot the misfit between model and observation as a function of these parameters, and find the best-fit model. The results are plotted in Figure 7.

The inversion identifies a NW-striking fabric. This could represent either an open fracture set with this orientation, or the maximum horizontal stress orientation (or a combination of both). The NW strike matches a fracture set identified from core and image analysis (Wilson and Monea, 2004). However, the dominant fracture set in core samples is a NE-striking set. An important question to ask is why the splitting has imaged this secondary fracture set, and not the principal set? In order to answer this question, and to increase our understanding of why events are located as they are, we construct a simple geomechanical model to simulate the evolution of stress during CO_2 injection.

Seismic observations and geomechanical modeling

Passive seismic activity represents an observable manifestation of geomechanical deformation in and around the reservoir. Therefore, passive seismic observations can be combined with geomechanical models to further enhance the understanding of the subsurface. In this section, we demonstrate how even simple geomechanical models can enhance seismic observations.

We generated a simplified coupled geomechanical/fluid-flow model, consisting of a flat, rectangular reservoir with much larger breadth than thickness, set in a homogenous overburden. The model explicitly couples a fluid-flow simulator (TEMPEST, Roxar Ltd.) with a finite element geomechanical solver (ELFEN, Rockfield Ltd.). A message passing interface (MPI) controls the transfer of pore pressures from TEMPEST to ELFEN, and of porosity and permeability changes caused by geomechanical deformation from ELFEN to TEMPEST. A typical pattern at Weyburn was modeled, with a horizontal injection well with a production well on either side. Symmetry arguments were used to reduce computational time, meaning that only a quarter of the reservoir was modeled. After eight years, a reduction in pore pressure from 15 to 11MPa was observed at the production wells, whilst pressures at the injector increased from 15–20MPa, approximating the pore pressure changes seen at Weyburn. Young's modulus for the reservoir was set to 12 GPa and Young's modulus for the overburden was set to 10 GPa in the immediate overburden and decreasing in stiffness towards the surface. This model can be considered a highly simplified representation of the Weyburn reservoir, matching the general geometry and properties, but missing much detail.

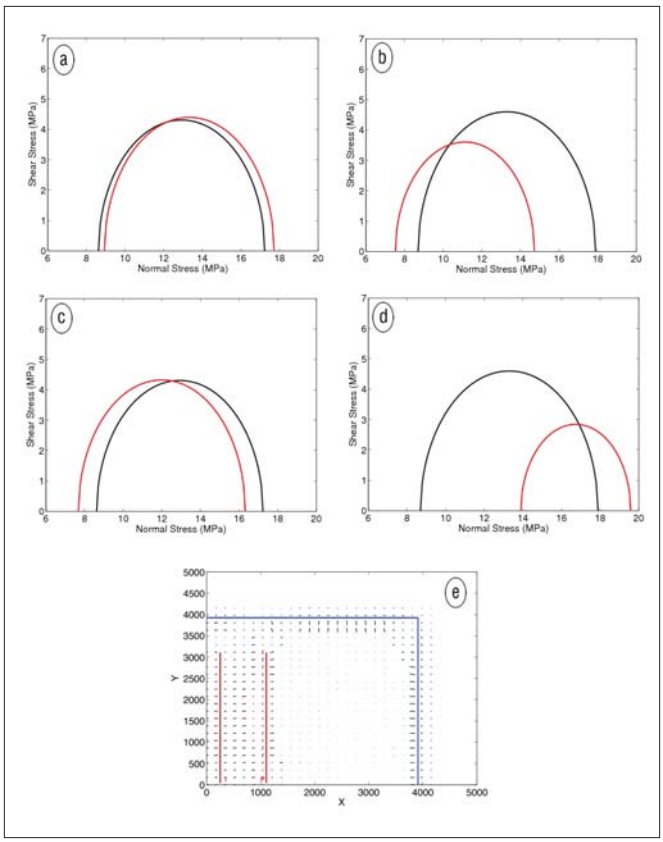

Figure 8. *Results from a simple geomechanical model representing the Weyburn reservoir. (a)–(d) Mohr circles showing the evolution of stress from the initial conditions (black) to postinjection conditions (red) in the overburden above the injection well (a), in the reservoir near the injection well (b), in the overburden above the producing well (c), and in the reservoir near the producing well (d). In (e) we model the stress-induced SWS fast directions (black ticks) for a vertically propagating S-wave, noting that the majority of fast directions are orientated perpendicular to the horizontal wells (marked in red).*

In Figure 8, we plot Mohr circles representing the stress evolution during injection at the injection (b) and production (d) wells, and in the overburden above these wells (a, c). The likelihood of failure (and therefore microseismicity) will be increased if the Mohr circle either translates to lower normal stresses, whilst maintaining its size (inducing shear failure), or if normal stresses increase such that pore collapse occurs. We note from Figure 8 that above, the production well, the Mohr circle translates to lower normal stresses with no decrease in deviatoric stress, increasing the likelihood of shear failure, whilst around the production well the Mohr circle translates to significantly higher normal stresses, increasing the likelihood of pore collapse. In contrast, around the injection well there is a decrease in deviatoric stress, whilst above the injection well there is a smaller increase in normal stress. The modeled stress evolution suggests that for this scenario, areas around and above the production wells will be placed at greater risk of failure than around the injector.

From Figure 3, we noted that, with the exception of the events induced by drilling activities in the injection well, the majority of events are located near the production wells to the

NW and SE of the injector. Without modeling, it is unclear why activity is not found around the injection well, where pore pressures are increasing, but is found around the production well, where pore pressures are decreasing, and in the overburden, where pore pressure changes will be small. However, the stress changes and the risk of failure inferred from the geomechanical model provide an explanation for why the events are located as they are. This highlights the need to link geomechanical models with indicators of deformation such as microseismic activity and/or surface deformation.

Changes in stress will also affect seismic velocities. In particular, seismic anisotropy can be highly stress-sensitive. Verdon et al. (2008) develop a model to compute the magnitude and orientation of shear-wave splitting induced by stress changes. For vertically propagating shear waves, the fast shear wave will align with the principal stress direction. In Figure 8e, we plot the SWS predicted by the geomechanical model, finding the fast direction becomes aligned perpendicular to the horizontal wells. This also matches the observations of splitting orientated to the NW (Figure 8), which is perpendicular to the NE-trending wells at Weyburn. This demonstrates another useful link between geomechanical modeling and seismic observation.

Discussion

The temporal clustering of microseismic events is episodic, which raises the question of what causes these discrete episodes of localized deformation. If the low-frequency events are interpreted as fluid movement, why do we only see them occasionally if fluid movement is occurring continuously? Focal mechanism analysis can provide information here. For example fluid movement would perhaps generate non-double-couple mechanisms. Focal mechanism analysis could also image the triaxial stress tensor in the reservoir. This is important information for guiding injection strategies and groundtruthing geomechanical models (e.g., Rutledge et al. 2004). However, focal mechanism analysis cannot be done with a single well array, and so has not been done for Weyburn.

It is gratifying that the events observed until November 2004 show good correlation with the time-lapse seismic results. However, not all negative amplitude anomalies seen in the time-lapse data have associated events. This perhaps indicates that although microseismicity has been observed to track CO_2 movement, the spatial and temporal distribution of microseismicity appears not to be a consistent mapping tool. However, with our limited array and paucity of seismicity, it is difficult to draw more firm conclusions about this.

Depth uncertainty in the location of microseismic events is a significant issue, especially when trying to ascertain that CO_2 is secure in the reservoir. The depth resolution can be improved very easily. Past experience suggests that extended vertical arrays, or multiwell arrays, would constrain depths to within roughly 10 m. Additionally, improved event location algorithms would better constrain depths, despite being more time consuming procedures.

Another important point is whether or not microseismicity above the reservoir indicates top-seal failure and the migration of CO_2 into the overburden. Stress arching effects can lead to failure in the over- and sideburden, without any fluid leaving the reservoir. To determine whether or not deformation results in increased fault permeability, it is necessary to consider the rheology of the rock with respect to the stresses at the time of faulting. This underscores the importance of having a good understanding of the potential geomechanical behavior of the storage site. However, it is likely that fault reactivation and topseal failure will be documented by a different spatial and temporal pattern in seismicity from those associated with stress arching effects.

A key question is: Should CCS operations always, often, or rarely employ passive seismic monitoring, and how should this decision be made? Downhole monitoring is now a commonly used tool for monitoring the hydraulic stimulation of fractures. It presents a low-cost option for long-term CCS monitoring. Ideally, such monitoring would record little induced seismicity. This would suggest that the CO_2 plume moves aseismically through the reservoir, inducing no significant rock failure, as seems to be the case at Weyburn. An important first step in such a monitoring project would be establishing the pre-injection level of seismicity. It is conceivable that passive seismic monitoring of CCS would be of limited use in areas with high amounts of natural seismicity. As Weyburn is the only CCS project to employ such monitoring, it is difficult to form more definitive conclusions. Our work also suggests that another important pre-injection step is the development of a good geomechanical model of the reservoir. Forward modeling can be then used to predict the seismicity associated with various injection scenarios.

Conclusions

We have presented the results of five years of passive seismic monitoring at the IEA GHG Weyburn CCS/EOR project. We have found that microseimicity rates correlate with periods of elevated CO_2 injection rates, and also with changes in production activities in nearby wells. The distribution of injection-related event locations also appears to correlate with the regions of CO_2 saturation that have been identified using 4D seismic. However, overall the rates of seismicity are low. The low rates of microseismicity indicate that the reservoir is not undergoing significant geomechanical deformation, which is encouraging in regard to security of storage.

We also demonstrate how shear-wave splitting measured on microseismic events can be used to identify structures such as aligned fractures in the reservoir, and confirm the presence of one of the fracture sets identified in core samples. This is not the dominant fracture set. However, geomechanical modeling shows that the evolution of stress during injection is likely to preferentially open this set, making it dominate the splitting results. Simple geomechanical modeling suggests that areas around and above production wells will be at greater risk of failure than around the injection well. This prediction matches the observed event locations, which are in general closer to production wells.

In future CCS projects, the avoidance of geomechani-

cal deformation is likely to be a key aim, and injection programs will probably be tailored to achieve this. The observations that can be made with passive seismic monitoring in this study revealed a low rate of seismicity. The result can be used to prove that geomechanical deformation is not occurring. When demonstrating security of storage it is equally as important to identify what is not happening (i.e., that there is no geomechanical activity), as it is to demonstrate what is happening. Passive seismic monitoring will provide a useful tool, and it is cost effective to run, requiring little in the way of maintenance and data processing. TLE

References

Rutledge, J. T., W. S. Phillips, and M. J. Mayerhofer, 2004, Faulting induced by forced fluid injection and fluid flow forced by faulting: An interpretation of Hydraulic-fracture microseismicity, Carthage Cotton Valley field, Texas, *Bulletin of the Seismological Society of America*, 94, 1817–1830.

White, D., 2009, Monitoring CO_2 storage during EOR at the Weyburn-Midale Field, *The Leading Edge*, 28, 838–842.

White D. J. and J. W. Johnson, 2008, Integrated Geophysical and Geochemical Monitoring Programs of the IEA GHG Weyburn-Midale CO_2 Monitoring and Storage Project, GHGT9 Proceedings, 2349–2356.

Wilson M., and M. Monea, eds. 2004, IEA GHG Weyburn CO_2 monitoring and storage project summary report 2000–2004, *http://www.ptrc.ca/weyburn_first.php*.

Verdon, J. P. and J.-M. Kendall, 2009, Constraining fracture geometry from shear-wave splitting measurements of passive seismic data, *Geophysical Journal International*, 179, 1245–1254.

Verdon, J. P., D. A. Angus, J. M. Kendall, and S. A. Hall, 2008, The effects of microstructure and nonlinear stress on anisotropic seismic velocities, Geophysics, 73, 4, D41–D51).

Acknowledgments: The authors thank the PTRC and the Weyburn field operator, EnCana, for making the passive seismic data available. James Verdon was funded by a UKERC Interdisciplinary Studentship. We are also grateful to the PTRC for funding. This work is part of the Bristol University Microseismicity Projects (BUMPS) and a contribution from the Bristol CO2 Group (BCOG). Shawn Maxwell and Marc Prince are acknowledged for their work on determination of microseismic hypocenters. Barbara Dietiker prepared some of the figures. We also thank the sponsors of the IPEGG consortium (BP, BG, StatoilHydro and ENI) and Rockfield Software (Martin Dutko) for support. Rockfield Software and Roxar Limited are thanked for providing copies of the ELFEN and TEMPEST software, respectively. Finally, we thank Tom Wilson for his helpful and constructive comments on the manuscript. Contribution 20090301 of the Geological Survey of Canada.

Corresponding author: james.verdon@bristol.ac.uk